Research Article | Vol. 31, No. 15 / 17 Jul 2023 / Optics Express 23877
Optics EXPRESS

Coherent terahertz laser feedback interferometry for hydration sensing in leaves

MAYURI KASHYAP,[1,2,3] JARI TORNIAINEN,[1] KARL BERTLING,[1] URBI KUNDU,[1,2,3] KHUSHBOO SINGH,[2] BOGDAN C. DONOSE,[1] TIM GILLESPIE,[1] YAH LENG LIM,[1] DRAGAN INDJIN,[4] LIANHE LI,[4] EDMUND H. LINFIELD,[4] A. GILES DAVIES,[4] PAUL DEAN,[4] MILLICENT SMITH,[5,6] SCOTT CHAPMAN,[5,6] APARAJITA BANDYOPADHYAY,[7] AMARTYA SENGUPTA,[2,3,8] AND ALEKSANDAR D. RAKIĆ[1,3,*]

[1]*School of Information Technology & Electrical Engineering, The University of Queensland, Brisbane QLD 4072, Australia*
[2]*Department of Physics, Indian Institute of Technology Delhi, New Delhi – 110016, India*
[3]*The University of Queensland – Indian Institute of Technology, Delhi Academy of Research (UQIDAR), India*
[4]*School of Electronic and Electrical Engineering, The University of Leeds, Leeds LS2 9JT, UK*
[5]*School of Agriculture and Food Sciences, The University of Queensland, Brisbane QLD 4072, Australia*
[6]*Queensland Alliance for Agriculture and Food Innovation, The University of Queensland, Brisbane QLD 4072, Australia*
[7]*DRDO-Industry-Academia Center of Excellence, Indian Institute of Technology Delhi, New Delhi – 110016, India*
[8]*a.rakic@uq.edu.au*
[*]*littlejxl@126.com*

Abstract: The response of terahertz to the presence of water content makes it an ideal analytical tool for hydration monitoring in agricultural applications. This study reports on the feasibility of terahertz sensing for monitoring the hydration level of freshly harvested leaves of *Celtis sinensis* by employing a imaging platform based on quantum cascade lasers and laser feedback interferometry. The imaging platform produces wide angle high resolution terahertz amplitude and phase images of the leaves at high frame rates allowing monitoring of dynamic water transport and other changes across the whole leaf. The complementary information in the resulting images was fed to a machine learning model aiming to predict relative water content from a single frame. The model was used to predict the change in hydration level over time. Results of the study suggest that the technique could have substantial potential in agricultural applications.

1. Introduction

Light, air, moisture, nutrients, and proper temperature constitute the basic requirements for healthy plants and play an important part in the photosynthetic process. An excessive or insufficient supply of any of these elements can subject the plants to stress, diseases, and low yield. Agriculture is largely responsible for sustaining the growing human population; therefore, the available land and water resources need to be efficiently managed to attain the required rates of productivity. The majority of the cultivated land (80%) is rain-fed; the remaining 20% is irrigated, but it is responsible for producing 40% of the food for the world [1]. With constant soil degradation, climate change effects, and water stress, primarily due to agriculture, understanding

#490217 https://doi.org/10.1364/OE.490217
Journal © 2023 Received 21 Mar 2023; revised 8 Jun 2023; accepted 8 Jun 2023; published 5 Jul 2023

Optics EXPRESS

the dynamics between plants and water thus becomes crucial to optimize crop yields by regulating the available resources as they become increasingly scarce.

The water content of plants has previously been measured using a variety of techniques, including visible [2] and near-infrared spectroscopy [2,3], mid-infrared spectroscopy [3], microwave resonators [4], nuclear magnetic resonance (NMR) based sensing [5,6] and thermal imaging [7] (see Jones [8] for a comprehensive review of capabilities and limitations of different techniques). Candidates for water content monitoring have also included Terahertz (THz) spectroscopy/imaging as a complementary technique, which uses the THz region of the electromagnetic spectrum (0.2–10 THz) to evaluate the water dynamics of plants, mainly as transmission through the leaves [9–15]. THz radiation has several properties that make it well suited for hydration level monitoring in agricultural and biomedical fields [16]. Because of its low energy, THz is non-ionizing, non-destructive, and is regarded as safe for biological materials. Furthermore, increased absorption of THz is observed in the presence of polar molecules such as water [17], which facilitates its application for hydration studies. In addition to the attenuation of THz radiation by atmospheric water vapour [18], absorption loss also occurs for materials with high liquid water content [19], which may pose practical limitations to the use of the technique. The majority of commercially available THz imaging systems are based on photoconductive antenna based time-domain and continuous wave spectrometers, while systems based on quantum cascade lasers (QCLs) are now being commercialised. All three technologies have their distinct utilities and limitations and have subsequently been used in hydration monitoring [20–24].

Biological materials often display non-homogeneity in their structure, formation and composition. The same is true for leaves, which differ in their physical and chemical characteristics depending on the species and exposure to the different abiotic factors required for their growth. However, such differences are also observed for leaves within the same plant [25] depending on the stage of maturity, canopy level and light exposure, which act as stress-stimuli and affect the thickness, texture, composition of the leaves. This, along with the heterogeneous structure of the leaf plays an important role in the distribution, utilization and retention of water, thus affecting the THz transmission loss [22,26] through it. Such variations may act as limiting factors for hydration studies using theoretical models because of the increment in the number of parameters involved for the approximations [23,27]. In order to address and utilise such variations for hydration analysis, this study focuses on generalising these differences with the aid of machine learning. Smart techniques have been integrated into the agricultural sector with the help of machine learning, particularly in managing yield, diseases, and resources such as soil, water, and livestock [28–30]. Due to intrinsic properties of THz, it has also been utilized in conjunction with machine learning for quantification, identification and quality control of agricultural produce [31–36] among others. In the current study, machine learning assists in the data processing to quantify the relative water content using a partial least squares regression (PLSR) model that takes into account dimensionality reduction and the collinearity of the information in variables with the mapped water content from various leaves.

The change in hydration of leaves is approximated using narrow-band, pulsed QCL-based laser feedback interferometry (LFI) imaging with leaf moisture content declining due to separation from the main plant. Coherent nature of the detection in LFI allows the extraction of amplitude-phase pairs for the material being sensed [37–39] (see Fig. 1). This allows the measurement of both reflectivity with absorption coefficient concurrently and when combined with a raster scanning mirror, individual complex pixels can be generated rapidly, allowing for high-resolution megapixel images generated in minutes [40]. The high-speed frame rate helps with the process of monitoring over time, including the change in plant hydration where small variations of voltage in the self-mixing signal [38] from the leaf indicate the underlying hydration dynamics. The high-resolution pixels from the LFI image frames were used to segment the leaves into lamina and veins, each of which has different morphological and physiological properties, and response

Optics EXPRESS

to drought stress. This segmentation, applied to both amplitude and phase images in the current work, as opposed to examining the leaf as a single entity, allowed for detailed feature extractions for approximating the hydration content in plants using the nested cross-validation and PLSR models. This led to improved prediction accuracy in hydration monitoring, which is discussed in depth in the following sections.

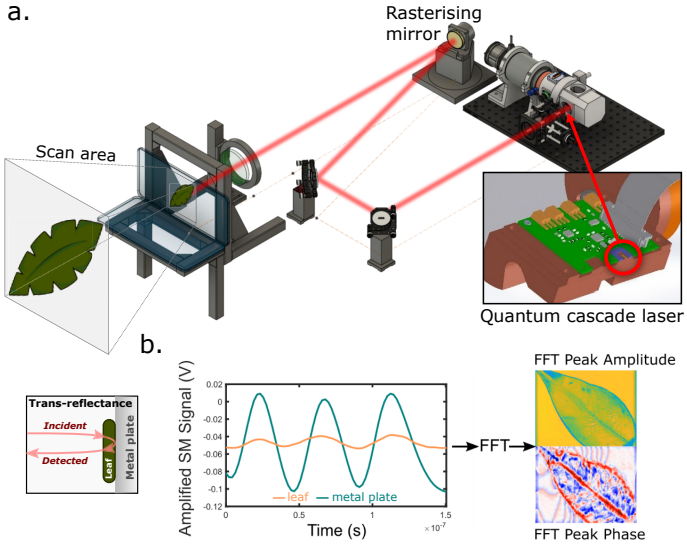

Fig. 1. a: Leaves were scanned using a quantum cascade laser and a rasterising mirror. **b:** The acquired self-mixing signal was amplified and FFT-transformed to produce terahertz amplitude and phase images of the sample.

2. Materials and methods

2.1. Leaf samples

This study used leaves collected from mature *Celtis sinensis* (also known as Chinese hackberry) plants located on the St Lucia Campus of the University of Queensland, Australia. The leaves were collected from the third axial positions in relation to the tip of the branch. The initial, fresh weight of the leaves were recorded within 10 minutes of harvest and LFI measurements were initiated within 30 minutes. In total, five leaves were analysed for water content. The leaves had a surface area of around 85 mm by 50 mm and a thickness in the order of 0.15 mm. Of these leaves, the third leaf (leaf 3), though fully-expanded, was observed to be younger as compared than the other leaves due to its lighter shade of green.

2.2. Pulsed LFI imaging platform

The LFI imaging platform based on QCL-THz used in this study (Fig. 1) has been described in detail by Lim et al. [40] and is thus, only briefly recapitulated here. The QCL chip is encased in a chamber that operates at 50 K using a Stirling cooler. The THz laser generated by this chip passes through a 30 mm collimating lens (Tsurupica, BBlaser Inc.), a set of 75 mm static reflecting mirrors, a 50 mm rasterising focusing mirror (Optics in Motion), through a 50 mm focusing lens (Tsurupica, BBlaser Inc.) which allows raster imaging of the scan area, as seen in Fig. 1(a). The resulting self-mixed interferometry signal is amplified, and Fourier-transformed to produce corresponding amplitude and phase values for the image pixels. Full specifications of the imaging platform can be found in Table 1.

Optics EXPRESS

Table 1. System parameters for LFI imaging setup.

System parameters	Fast THz –QCL–LFI
Frequency	2.8 THz with 600 MHz Freq. Sweep
Output power	2 mW peak
Image scan area	60 (H) × 40 (V) mm^2
Image pixel area	1200 (H) × 400 (V) (0.48 M pixels)
Pixel size	50 (H) × 100 (V) µm
Image acquisition time	3 min 20 Seconds (Mechanically Limited)

LFI is one of the most basic, yet compact sensing techniques where the emitter also serves as a highly sensitive detector [41–43]. In sensing applications, the combination of QCLs and LFI is particularly advantageous, especially in the THz band, where there is a scarcity of external detectors that offer both high-speed and high-sensitivity [38]. Indeed, LFI with THz QCLs — which possess high output power, low phase-noise and stability under optical feedback — has been successfully employed for sensing [40,44–47] and benefits from the intrinsic advantages inherent to homodyning detectors, in particular suppression of unwanted background radiation. The use of the QCL itself as the detector means that the detection speed is theoretically limited only by the device itself [48,49].

2.3. Imaging procedure

During imaging, the ventral side of the leaf was fixed to a metal plate so that the adaxial stomatal pores were not blocked to ensure gas exchange. The metal plate was attached to a 0.1 mg precision electronic balance (JF2104, Jinnuo, Zhejiang, China), allowing for simultaneous weighing of the leaf. Leaves were imaged for approximately 10 hours in a transflectance mode while also recording the leaf weight for each frame. All measurements were conducted in a climate-controlled optics laboratory on a vibration-compensated optical bench. Both the relative humidity and room temperature were recorded at the beginning of each imaging sequence (relative humidity 50% ± 6%, room temperature 23 °C ± 2 °C).

3. Image processing and water content prediction

Each measured frame produced corresponding amplitude and phase images, which required some preprocessing before water content could be determined. As the amplitude images are affected by the ambient temperature, each frame had to first be normalized to a common reference in order to enable comparison between different time points and individual leaves. Thus, the median amplitude of the metal backplate in each frame was used as a reference standard for normalising the amplitude values. Exemplar-produced images can be seen in Fig. 2 and Fig. 3(a).

The phase images produced by the imaging platform were phase wrapped (Fig. 3(b)) and had to first be resolved using the robust two-dimensional unweighted unwrapping [50]. The unwrapped phase images were then gradient corrected by subtracting a heavily smoothed version of the original frame in order to account for varying optical path length over the scanned area. Finally, frames containing obvious imaging artifacts were manually removed at this stage (approximately 1% – 5% of the total frames). A 3D render generated by combining a stack of all the frames of the third leaf (leaf 3) is shown in Fig. 2(a) (generated using ImageJ [51], Materialize by Bounding Box Software, and Blender [52]). This approach allows observing microscopic features, such as stomata and leaf vascular system, by assigning an alpha channel (transparency) to the rest of the leaf (light green) and dark tone to the highly hydrated domains. The water transport process of the leaf is visualized at individual slice level in Fig. 2(b–d). A time lapse movie highlighting hydration levels in a leaf over 360 minutes is presented in Visualization 1.

Optics EXPRESS

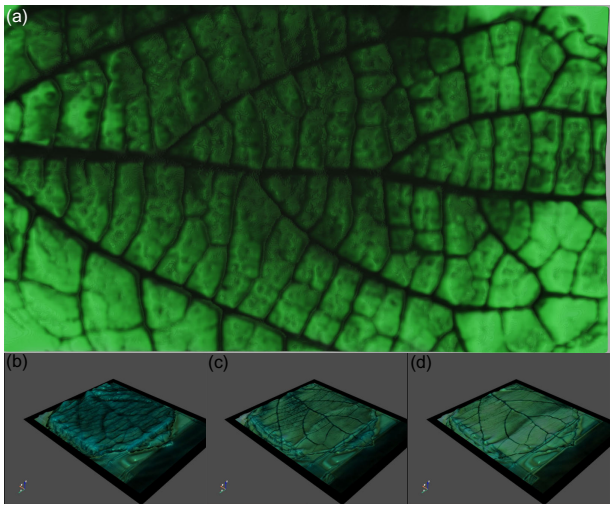

Fig. 2. **(a)** Top-view of a 3D leaf render composed of all the measured frames of leaf 3. **(b–d)** Topographical representation of water transport over the leaf at (b) t=0 mins, (c) t=180 mins, (d) t=360 mins. Visualization 1 shows the progression of this leaf over the entire 360 mins.

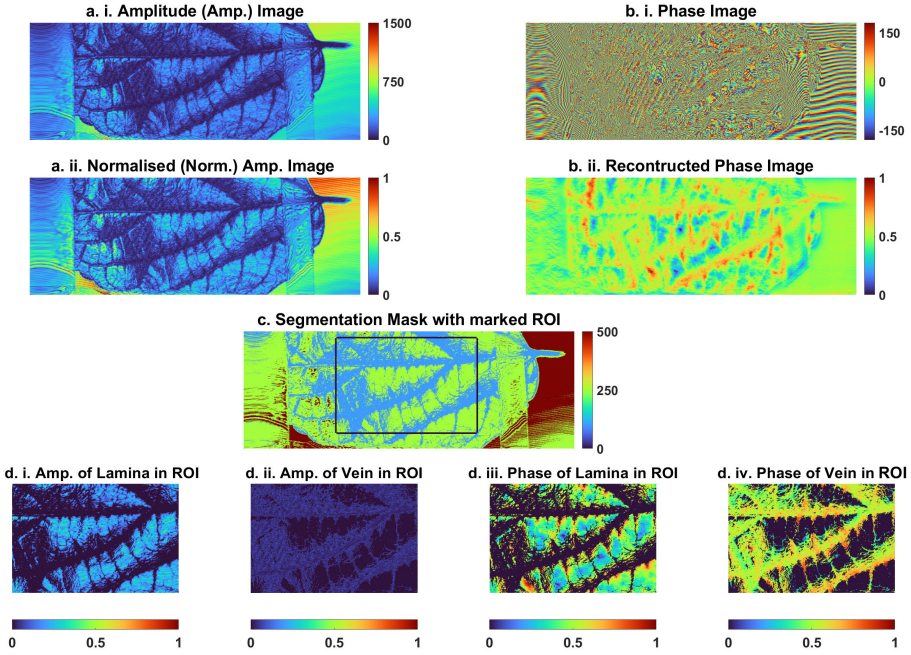

Fig. 3. Image preprocessing pipeline for amplitude and phase images. **a.i:** Raw amplitude image of a leaf taped on a metal plate. **a.ii:** Amplitude image normalized to the amplitude of the metal plate. **b.i:** Raw phase image of the leaf. **b.ii:** Phase unwrapped and gradient-filtered phase image. **c:** Segmentation mask for selecting pixels belonging to veins (blue), lamina (green) and metal (red). The black box indicates the region of interest (ROIs) used for further analysis steps. **d.i-iv:** Amplitude and phase maps for segmented lamina and vein ROIs. Visualization 2 shows the segmentation process for the leaf over 8 hours.

Optics EXPRESS

Pixels in each frame were segmented into one of three classes (background, lamina, and vein). Segmentation was performed using Otsu's variance-based multi-thresholding [53] by using the amplitude image as an input (Fig. 3(c)). The resulting segmentation mask was used for both amplitude and phase images in the later processing steps. Finally, a 200×200 pixels region-of-interest (ROI) was selected near the central vein of each leaf (Fig. 3(d)). The purpose of the ROI-based analysis was to ensure that the varying size between the leaves and the presence of non-leaf objects (metal plate, parts of the sample holder, adhesive tape, etc.) would not confound the analysis. Visualization 2 shows the segmentation process for leaf 2 over 8 hours with amplitude and phase maps for the segmented lamina and vein ROIs.

The relative moisture content (RMC) predictor was constructed by training a partial least squared regression (PLSR) model using the data from the first 8 hours of each measurement. The dependent variable (i.e., RMC) of the model was determined as the relative mass loss of the leaf, where the value 1.0 corresponded to the weight of a freshly harvested leaf and the value of 0.05 to the weight of the dried leaf. In order to denoise the dependent variable, the measured weight-over-time was smoothed with a Savitzky-Golay filter. Independent variables of the model were extracted from the segmented lamina and vein regions of the amplitude and phase images within the specified ROIs (Fig. 4(a)). Extracted features with more than 85% correlation with the RMC were aggregated into a feature vector. To account for the differences in ambient conditions, temperature and relative humidity of the laboratory were also included as two extra features.

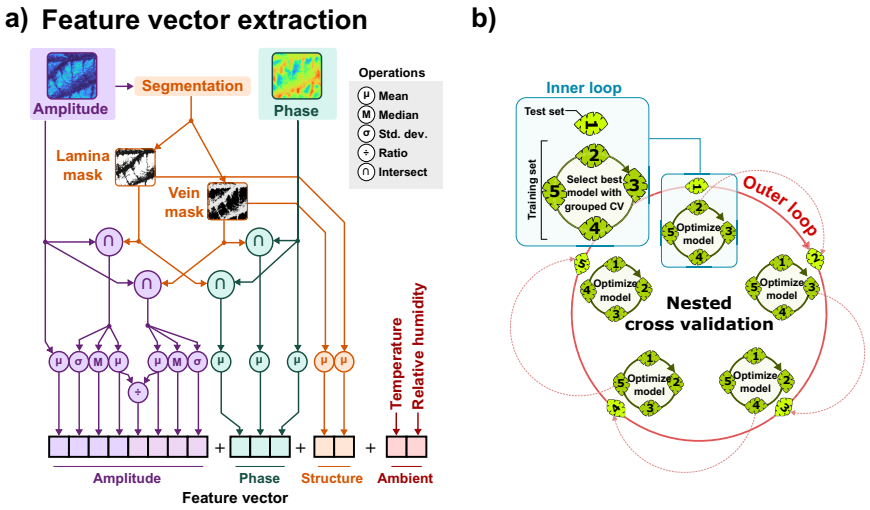

Fig. 4. **a:** The feature vector used for predicting RMC was constructed by combining the descriptive statistic and segmentation masks of amplitude and phase images within the region of interest. In addition, relative humidity and temperature were added to the feature vector as ambient variables. **b:** Performance of RMC prediction was evaluated using nested cross-validation. In nested CV, each individual leaf was sequentially used as a test set while the remaining leaves were used to train the regression model.

The prediction accuracy of the model was tested with nested cross-validation (CV) (Fig. 4(b)). Within each iteration, the number of components in the PLSR model was optimized using training samples from four leaves, leaving the fifth leaf for testing. This process was then repeated for each individual leaf. Model performance is reported for both the inner and outer loops of the CV in terms of Pearson's correlation (R), coefficient of determination (R^2), and root mean squared error (RMSE).

The `scikit-learn` module [54] of Python3 was used to train and evaluate the PLSR models.

Optics EXPRESS

4. Results

For three of the five leaves, the change in normalised amplitude of the lamina over time points 90, 240, and 360 minutes after plucking is shown in Fig. 5. Visualization 3 shows the change in amplitude and phase for leaf 3. As a response to water deficit, shrinking of the leaf surface, uneven dynamics of moisture distribution, and the difference between the drying periods of lamina and veins, and between secondary and primary veins can be observed in this visualisation.

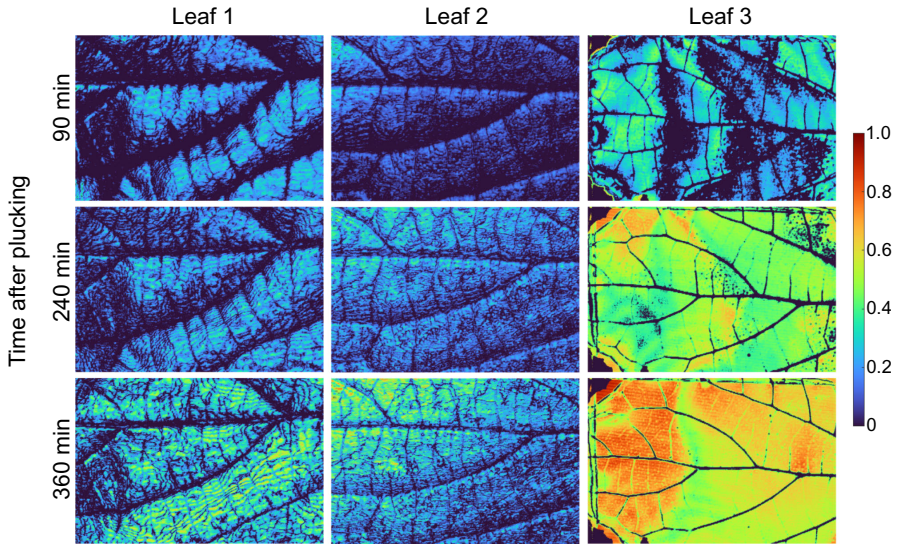

Fig. 5. Change in reflectance through lamina after 90, 240 and 360 minutes (min) after being harvested for three leaves. Visualization 3 shows the change in amplitude and phase for leaf 3.

Accuracy metrics of the PLSR model for predicting RMC are collected in Table 2 with the best results highlighted. The test set accuracy for predicting RMC was R^2=0.58–0.88 and RMSE=0.05–0.16. The predicted and measured RMC values also exhibited a strong linear correlation (R = 0.92–0.96). Residuals of the predictions were relatively uniform over the 8-hour measurement period.

Table 2. Parameterised regression errors with best results highlighted.

	Inner Loop					Outer Loop		
	RMSE_{cv}	R^2_{cv}	R_{train}	RMSE_{train}	R^2_{train}	RMSE_{test}	R_{test}	R^2_{test}
Leaf 1	0.12	0.78	0.89	0.12	0.79	−0.05	0.94	0.66
Leaf 2	0.12	0.77	0.88	0.12	0.78	0.08	−0.96	0.67
Leaf 3	−0.09	−0.85	−0.92	−0.09	−0.85	0.16	0.92	0.67
Leaf 4	−0.09	−0.85	−0.93	−0.09	−0.86	0.16	−0.96	0.58
Leaf 5	0.12	0.72	0.85	0.12	0.73	0.09	0.95	−0.88

Graphical representations of the results are shown in Fig. 6 where the plot in the top row shows how the predicted RMC spreads in comparison to the true RMC limited by RMSE. The middle row shows the true or actual RMC calculated using the normalised weight, contrasted with the predicted RMC using the PLSR model. The predicted points lie close to the regressed diagonal line with disparities visible in a few predictions, including for the young leaf, leaf 3 and leaf 4. For the same leaves, as time progresses, the scatter plot of the predicted values is projected over

Optics EXPRESS

the line of true RMC in the bottom row of the figure. Since the leaf mentioned in the label is not used during the nested CV training, the predictions are not influenced by its features, making the predictions independent and unbiased in nature.

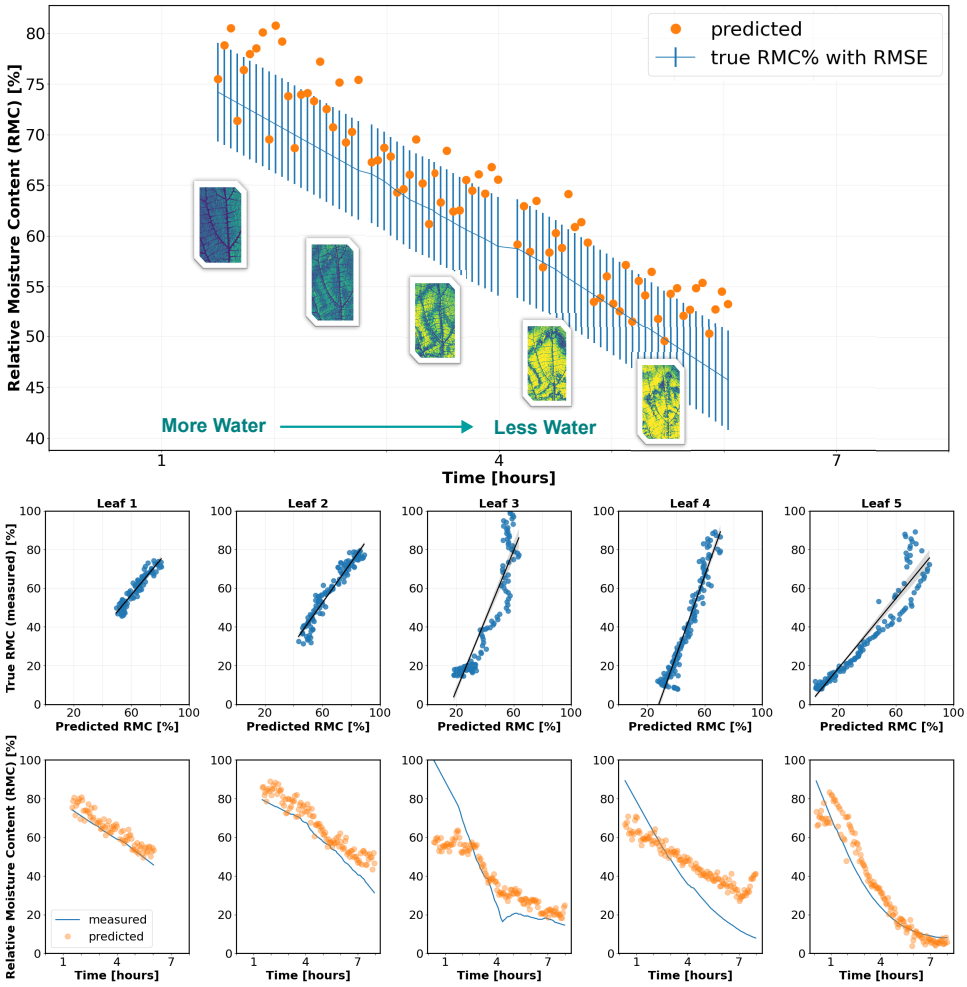

Fig. 6. Regression results for the PLSR model. The top row shows the prediction results for leaf 1 with the predicted values in comparison to the calculated RMSE for the prediction. The middle row displays the distribution of the true vs predicted values, while the bottom row shows the corresponding scatter plot of the predicted RMC values over time with respect to the true RMC values. Insets in the bottom row of leaf 1 show how the THz amplitude image alters with corresponding time points as the leaf dries out.

5. Discussion

In vascular plants, the leaf serves as the primary locus for both photosynthesis and transpiration. Its formation, development, and biological and physiological traits are influenced by a number of abiotic factors, including temperature, light, moisture, and others. These factors affect the growth pattern of the leaves and are responsible for variations in the cross-section, structure, and properties of leaves within the same species, plant or branch [25]. This variation can be observed in Fig. 5 where leaf 1 and leaf 2 are not identical even when they show fully matured leaves

Optics EXPRESS

from the same plant. leaf 3, on the other hand, is a young, fully expanded leaf from the third apical position. However, since it is younger than the other leaves, there is a difference in the cross-section area. The lamina is thinner than the other leaves, evident from the higher amplitude through the lamina even at 90 minutes. Also, the girth of the veins is observed to be smaller than those of leaf 1 and leaf 2. The left-hand side corners of leaf 3 frames were identified as metal-backing and were excluded using the automated processing algorithm.

Because of transpiration, the moisture inside the leaves decreases over time, reducing THz absorption through the leaf. This results in a change of phase and increase of amplitude through the leaf as the THz passes through it, reflecting from the metal-backing and through the leaf again. Along with this, the thickness of the veins decreases as can be observed in Fig. 5. The protruding veins on the dorsal side of the leaf prevent the leaf to be observed on the same focal plane. The extent of protrusion or the thickness of the veins also impacts the imaging of the lamina as it forms an angle at its connection to the midrib and the smaller veins. As the leaf dries, the veins become thin and the angle also reduces, allowing the lamina to lay flatter on the metal backing. The leaves also start curling from the outer edges to limit the water loss. For the current work, however, since the leaves are lightly fixed to the backing, either with a magnetic frame or tape, the leaves are stretched and do not completely curl up, but while monitoring the complete frame, the edges are observed to shrink, reducing the area covered by the leaf over time. The thinning of the veins can also be observed using the phase images Visualization 2 and Visualization 3 where the phase difference between the lamina and the veins decreases over time as the veins flatten out and the moisture content in them reduces.

On a closer inspection of the leaves, leaf 2 and leaf 3 in Fig. 5 and Visualization 3 show the presence of stomata in the form of small round spots, more prominent in leaf 3. Stomata are found in abundance in young leaves, but as they mature, the stomatal density decreases with the increase in leaf size, while the stomatal conductance increases [55,56]. This, along with the thickness and degree of flatness in a young leaf, allows visibility of stomata in the young leaves with better focus as compared to matured leaves. This provides the scope of utilizing the high-resolution LFI imaging setup for monitoring the growth stage of plants.

Nested CV for the RMC produces prediction errors (i.e., RMSE) in the range of 5% – 16% indicating the error level to be anticipated for untested sets. The R^2, on the other hand, supports the contribution of the selected features for the prediction model. Predicted water content values for leaves 1, 2, and 5, closely matched the measured values over all time points. With leaves 3 and 4, however, the rate of dehydration was biased although the general trend was still correct.

This study utilized previously established double transmission measurement mode [24] which was implemented by placing a highly reflective metal back-plate behind the imaged leaf. The double transmission mode increases the SNR of the acquired LFI signal, thus boosting the contrast of the resulting THz image. It should be noted, however, that since the use of a metal back-plate might not be feasible in real-world applications, the technique still works without it albeit with slightly impaired contrast.

The use of harvested leaves rather than leaves attached to a plant is one of the major limitations of the current study. In contrast to the study of *in-vivo* leaves, the drop in water content of harvested leaves is rapid and constantly decreasing. As such, the experiment would need to be replicated with live plants in the future. Secondly, it was observed that changes in both relative humidity and temperature across different measurements can seriously hamper prediction accuracy if not accounted for. This is most likely due to humidity and temperature influencing both leaf dehydration and the quality of the THz signal. Humidity and temperature were, therefore, included as an additional feature pair for each measured frame in this study. The environmental variables, however, were only measured at the start of each measurement and were not monitored throughout the experiment. It is possible that constant monitoring of the ambient conditions could improve the model's robustness even further. Finally, reference methods other than relative

Optics EXPRESS

mass could be used to model water transport more realistically. For this study, mass was chosen for practical reasons due to its integrability with the imaging platform and the optical bench.

This study focused on monitoring the bulk hydration level of leaves. This limitation was imposed by the reference analysis method, which could only measure weight loss across the entire leaf. The resulting THz images, on the other hand, showed shifting contrast within the leaves, which could be attributed to the internal reorganisation of available water over time instead of a steady and evenly distributed decrease in moisture. Therefore, in addition to predicting the total amount of water, QCL-THz imaging could be able to map the actual water transport dynamics.

6. Conclusion

Hydration level monitoring is a very significant issue for the agriculture sector as irrigation resources are starting to dwindle. Estimating the exact prediction accuracy required for hydration level monitoring is nontrivial, but it's plausible that the QCL-THz imaging technique used in this study could be well suited for the task. The QCL-THz technique also has appealing features compatible with agriculture, since it is a non-destructive imaging technique capable of producing high-resolution images with relatively high frame rates.

A combination of image processing, feature extraction, and machine learning was used to establish the relationship between the THz images and RMC in the leaves. The model was trained using selected features extracted from both amplitude and phase images to predict the RMC, which was possible due to the features extracted from the frames acquired with sufficiently high-resolution. Fast acquisition of THz images of the leaves under water stress also shows a redistribution pattern of available water which could be developed further to understand the biochemical features of the leaf. High resolution also allowed the observation of stomata in young leaves, which could be utilized for maturity monitoring during harvesting. A similar model could also potentially be implemented with convolutional neural networks, although the approach would require significantly more independent samples than the current study.

Funding. Engineering and Physical Sciences Research Council (EP/T034246/1, EP/W028921/1); Department of Atomic Energy, Government of India (37(3)/14/01/2016-BRNS/37015); Defence Research and Development Organisation (DFTM/03/3203/M/01/JATC); Australian Research Council (DP200101948, DP210103342).

Disclosures. The authors declare no conflicts of interest.

Data availability. Data underlying the results presented in this paper are not publicly available at this time but may be obtained from the authors upon reasonable request.

References

1. FAO, *The State of the World's Land and Water Resources for Food and Agriculture – Systems at breaking point (SOLAW 2021)* (FAO, 2021).
2. X. Jin, C. Shi, C. Y. Yu, T. Yamada, and E. J. Sacks, "Determination of leaf water content by visible and near-infrared spectrometry and multivariate calibration in Miscanthus," Front. Plant Sci. **8**, 1–8 (2017).
3. E. R. Hunt and B. N. Rock, "Detection of changes in leaf water content using Near- and Middle-Infrared reflectances," Remote. Sens. Environ. **30**(1), 43–54 (1989).
4. M. I. Menzel, S. Tittmann, J. Bühler, S. Preis, N. Wolters, S. Jahnke, A. Walter, A. Chlubek, A. Leon, N. Hermes, A. Offenhäuser, F. Gilmer, P. Blümler, U. Schurr, and H. J. Krause, "Non-invasive determination of plant biomass with microwave resonators," Plant, Cell and Environment **32**(4), 368–379 (2009).
5. C. W. Windt, M. Nabel, J. Kochs, S. Jahnke, and U. Schurr, "A mobile nmr sensor and relaxometric method to non-destructively monitor water and dry matter content in plants," Front. Plant Sci. **12**, 617768 (2021).
6. A. Merchant, M. R. Smith, and C. W. Windt, "In situ pod growth rate reveals contrasting diurnal sensitivity to water deficit in Phaseolus vulgaris," J. Exp. Bot. **73**(11), 3774–3786 (2022).
7. I. Leinonen and H. G. Jones, "Combining thermal and visible imagery for estimating canopy temperature and identifying plant stress," J. Exp. Bot. **55**(401), 1423–1431 (2004).
8. H. G. Jones, "Irrigation scheduling: Advantages and pitfalls of plant-based methods," J. Exp. Bot. **55**(407), 2427–2436 (2004).
9. Z. Gong, D. Deng, X. Sun, J. Liu, and Y. Ouyang, "Non-destructive detection of moisture content for ginkgo biloba fruit with terahertz spectrum and image: A preliminary study," Infrared Phys. & Technol. **120**, 103997 (2022).
10. Z. Zang, Z. Li, X. Lu, J. Liang, J. Wang, H.-L. Cui, and S. Yan, "Terahertz spectroscopy for quantification of free water and bound water in leaf," Comput. Electron. Agric. **191**, 106515 (2021).

Optics EXPRESS

11. A. K. Singh, A. V. Pérez-López, J. Simpson, and E. Castro-Camus, "Three-dimensional water mapping of succulent agave victoriae-reginae leaves by terahertz imaging," Sci. Rep. **10**(1), 1–9 (2020).
12. B. Breitenstein, M. Scheller, M. K. Shakfa, T. Kinder, T. Müller-Wirts, M. Koch, and D. Selmar, "Introducing terahertz technology into plant biology: A novel method to monitor changes in leaf water status," Journal of Applied Botany and Food Quality **84**(2), 158 (2012).
13. S. Hadjiloucas, L. S. Karatzas, and J. W. Bowen, "Measurements of leaf water content using terahertz radiation," IEEE Trans. Microwave Theory Tech. **47**(2), 142–149 (1999).
14. D. M. Mittleman, R. H. Jacobsen, and M. C. Nuss, "T-ray imaging," IEEE J. Sel. Top. Quantum Electron. **2**(3), 679–692 (1996).
15. B. B. Hu and M. C. Nuss, "Imaging with terahertz waves," Opt. Lett. **20**(16), 1716–1718 (1995).
16. E. Castro-Camus, M. Koch, and D. M. Mittleman, "Recent advances in terahertz imaging: 1999 to 2021," Appl. Phys. B **128**(1), 12 (2022).
17. D. M. Mittleman, "Twenty years of terahertz imaging," Opt. Express **26**(8), 9417–9431 (2018).
18. M. van Exter, C. Fattinger, and D. Grischkowsky, "Terahertz time-domain spectroscopy of water vapor," Opt. Lett. **14**(20), 1128 (1989).
19. F. Novelli, B. Guchhait, and M. Havenith, "Towards intense thz spectroscopy on water: Characterization of optical rectification by gap, oh1, and dstms at opa wavelengths," Materials **13**(6), 1311 (2020).
20. R. Gente, N. Born, N. Voß, W. Sannemann, J. Léon, M. Koch, and E. Castro-Camus, "Determination of leaf water content from terahertz time-domain spectroscopic data," J. Infrared, Millimeter, Terahertz Waves **34**(3-4), 316–323 (2013).
21. L. Baldacci, M. Pagano, L. Masini, A. Toncelli, G. Carelli, P. Storchi, and A. Tredicucci, "Non-invasive absolute measurement of leaf water content using terahertz quantum cascade lasers," Plant Methods **13**(1), 51 (2017).
22. A. Afsharinejad, A. Davy, and M. Naftaly, "Variability of terahertz transmission measured in live plant leaves," IEEE Geosci. Remote Sensing Lett. **14**(5), 636–638 (2017).
23. M. Kashyap, A. Bandyopadhyay, K. Bertling, A. Sengupta, and A. D. Rakić, "Quantifying relative moisture content in dielectric models using cw-thz spectroscopy and supervised machine learning regression," in *Terahertz Emitters, Receivers, and Applications XII*, vol. 11827 (SPIE, 2021), p. 1182704.
24. K. Singh, A. Bandyopadhyay, K. Bertling, Y. L. Lim, T. Gillespie, D. Indjin, L. Li, E. H. Linfield, A. G. Davies, P. Dean, A. D. Rakic, and A. Sengupta, "Comparison of physical and system factors impacting hydration sensing in leaves using terahertz time-domain and quantum cascade laser feedback interferometry imaging," Sensors **23**(5), 2721 (2023).
25. L. K. Lauderbaugh and C. D. Holder, "The biomechanics of leaf oscillations during rainfall events," J. Exp. Bot. **73**(4), 1139–1154 (2022).
26. Z. Song, S. Yan, Z. Zang, Y. Fu, D. Wei, H.-L. Cui, and P. Lai, "Temporal and spatial variability of water status in plant leaves by terahertz imaging," IEEE Trans. Terahertz Sci. Technol. **8**(5), 520–527 (2018).
27. J. Helminiak, M. Alfaro-Gomez, G. G. Hernandez-Cardoso, M. Koch, and E. Castro-Camus, "Temperature dependence of the dielectric function of dehydrated biological samples in the thz band," Biomed. Opt. Express **14**(4), 1472–1479 (2023).
28. L. Benos, A. C. Tagarakis, G. Dolias, R. Berruto, D. Kateris, and D. Bochtis, "Machine learning in agriculture: A comprehensive updated review," Sensors **21**(11), 3758 (2021).
29. A. Goap, D. Sharma, A. Shukla, and C. Rama Krishna, "An iot based smart irrigation management system using machine learning and open source technologies," Comput. Electron. Agric. **155**, 41–49 (2018).
30. M. Roy Choudhury, S. Das, J. Christopher, A. Apan, S. Chapman, N. W. Menzies, and Y. P. Dang, "Improving biomass and grain yield prediction of wheat genotypes on sodic soil using integrated high-resolution multispectral, hyperspectral, 3d point cloud, and machine learning techniques," Remote Sens. **13**(17), 3482 (2021).
31. H. Zhang, Z. Li, T. Chen, and J.-J. Liu, "Detection of poisonous herbs by terahertz time-domain spectroscopy," J. Appl. Spectrosc. **85**(1), 197–202 (2018).
32. P. Nie, F. Qu, L. Lin, T. Dong, Y. He, Y. Shao, and Y. Zhang, "Detection of water content in rapeseed leaves using terahertz spectroscopy," Sensors **17**(12), 2830 (2017).
33. Y. Jiang, G. Li, H. Ge, F. Wang, L. Li, X. Chen, M. Lu, and Y. Zhang, "Machine learning and application in terahertz technology: A review on achievements and future challenges," IEEE Access **10**, 53761–53776 (2022).
34. J. Zhang, Y. Yang, X. Feng, H. Xu, J. Chen, and Y. He, "Identification of bacterial blight resistant rice seeds using terahertz imaging and hyperspectral imaging combined with convolutional neural network," Front. Plant Sci. **11**, 821 (2020).
35. R. Gente and M. Koch, "Monitoring leaf water content with THz and sub-THz waves," Plant Methods **11**(1), 15 (2015).
36. Y. Abautret, D. Coquillat, M. Lequime, M. Zerrad, and C. Amra, "Analysis of the multilayer organization of a sunflower leaf during dehydration with terahertz time-domain spectroscopy," Opt. Express **30**(21), 37971–37979 (2022).
37. S. Donati, "Developing self-mixing interferometry for instrumentation and measurements," Laser Photonics Rev. **6**(3), 393–417 (2012).
38. A. Rakić, T. Taimre, K. Bertling, Y. Lim, P. Dean, A. Valavanis, and D. Indjin, "Sensing and imaging using laser feedback interferometry with quantum cascade lasers," Appl. Phys. Rev. **6**(2), 021320 (2019).

Optics EXPRESS

39. P. Dean, J. Keeley, Y. L. Lim, K. Bertling, T. Taimre, P. Rubino, D. Indjin, and A. Rakic, *Mid-Infrared and Terahertz Quantum Cascade Lasers* (Cambridge University Press, 2023), chap. 15 Self-Mixing in Quantum Cascade Lasers: Theory and Applications, p. 477.
40. Y. L. Lim, K. Bertling, T. Taimre, T. Gillespie, C. Glenn, A. Robinson, D. Indjin, Y. Han, L. Li, E. H. Linfield, A. G. Davies, P. Dean, and A. D. Rakić, "Coherent imaging using laser feedback interferometry with pulsed-mode terahertz quantum cascade lasers," Opt. Express **27**(7), 10221–10233 (2019).
41. T. Taimre, M. Nikolić, K. Bertling, Y. L. Lim, T. Bosch, and A. D. Rakić, "Laser feedback interferometry: a tutorial on the self-mixing effect for coherent sensing," Adv. Opt. Photonics **7**(3), 570–631 (2015).
42. J. Keeley, K. Bertling, P. L. Rubino, Y. L. Lim, T. Taimre, X. Qi, I. Kundu, L. H. Li, D. Indjin, A. D. Rakić, E. H. Linfield, A. G. Davies, J. Cunningham, and P. Dean, "Detection sensitivity of laser feedback interferometry using a terahertz quantum cascade laser," Opt. Lett. **44**(13), 3314–3317 (2019).
43. K. Bertling, X. Qi, T. Taimre, Y. L. Lim, and A. D. Rakić, "Feedback regimes of lfi sensors: Experimental investigations," Sensors **22**(22), 9001 (2022).
44. S. Han, K. Bertling, P. Dean, J. Keeley, A. D. Burnett, Y. L. Lim, S. P. Khanna, A. Valavanis, E. H. Linfield, A. G. Davies, D. Indjin, T. Taimre, and A. D. Rakic, "Laser feedback interferometry as a tool for analysis of granular materials at terahertz frequencies: Towards imaging and identification of plastic explosives," Sensors **16**(3), 352 (2016).
45. K. Bertling, S. Han, T. Wu, C. Zhao, Y. L. Lim, P. Dean, S. P. Khanna, D. Indjin, E. H. Linfield, A. G. Davies, S. J. Wilson, T. Taimre, and A. D. Rakic, "Determining ethanol content of liquid solutions using laser feedback interferometry with a terahertz quantum cascade laser," IEEE Sens. Lett. **2**(3), 1–4 (2018).
46. K. Singh, A. Bandyopadhyay, K. Bertling, Y. L. Lim, T. Gillespie, A. Robinson, D. Indjin, Y. Han, L. Li, E. H. Linfield, A. G. Davies, P. Dean, A. D. Rakic, and A. Sengupta, "Monitoring water dynamics in plants using laser feedback interferometry," in *2020 Conference on Lasers and Electro-Optics Pacific Rim (CLEO-PR)*, (2020), pp. 1–2.
47. A. Bandyopadhyay, K. Bertling, D. Garg, K. Singh, T. Gillespie, Y. L. Lim, L. Li, P. Dean, D. Indjin, E. H. Linfield, A. G. Davies, A. D. Rakic, and A. Sengupta, "Sub-surface damage detection in marble structures using THz time domain and laser feedback interferometric imaging," in *Optics for Arts, Architecture, and Archaeology VIII*, vol. 11784 H. Liang and R. Groves, eds., International Society for Optics and Photonics (SPIE, 2021), p. 117840T.
48. G. Agnew, A. Grier, T. Taimre, K. Bertling, Y. L. Lim, Z. Ikonić, P. Dean, A. Valavanis, D. Indjin, and A. D. Rakić, "Frequency tuning range control in pulsed terahertz quantum-cascade lasers: Applications in interferometry," IEEE J. Quantum Electron. **54**(2), 1–8 (2018).
49. X. Qi, K. Bertling, T. Taimre, G. Agnew, Y. L. Lim, T. Gillespie, A. Demić, P. Dean, L. H. Li, E. H. Linfield, A. G. Davies, D. Indjin, and A. D. Rakić, "Terahertz quantum cascade laser under optical feedback: effects of laser self-pulsations on self-mixing signals," Opt. Express **29**(24), 39885–39894 (2021).
50. D. C. Ghiglia and L. A. Romero, "Robust two-dimensional weighted and unweighted phase unwrapping that uses fast transforms and iterative methods," J. Opt. Soc. Am. A **11**(1), 107–117 (1994).
51. C. A. Schneider, W. S. Rasband, and K. W. Eliceiri, "Nih image to imagej: 25 years of image analysis," Nat. Methods **9**(7), 671–675 (2012).
52. B. O. Community, *Blender - a 3D modelling and rendering package*, Blender Foundation, Stichting Blender Foundation, Amsterdam (2018).
53. N. Otsu, "A threshold selection method from gray-level histograms," IEEE Trans. Syst., Man, Cybern. **9**(1), 62–66 (1979).
54. F. Pedregosa, G. Varoquaux, A. Gramfort, V. Michel, B. Thirion, O. Grisel, M. Blondel, P. Prettenhofer, R. Weiss, V. Dubourg, J. Vanderplas, A. Passos, D. Cournapeau, M. Brucher, M. Perrot, and E. Duchesnay, "Scikit-learn: Machine learning in Python," Journal of Machine Learning Research **12**(85), 2825–2830 (2011).
55. H. Reed and E. Hirano, "The density of stomata in citrus leaves," Journal of Agricultural Research **43**, 209–222 (1931).
56. J. R. England and P. M. Attiwill, "Changes in stomatal frequency, stomatal conductance and cuticle thickness during leaf expansion in the broad-leaved evergreen species, eucalyptus regnans," Trees **25**(6), 987–996 (2011).